Materialia 17 (2021) 101124

Contents lists available at ScienceDirect

Materialia

journal homepage: www.elsevier.com/locate/mtla

Full Length Article

The effects of free surfaces on deformation twinning in HCP metals

B. Leu [a,*], M. Arul Kumar [b], I.J. Beyerlein [a,c]

[a] Materials Department, University of California Santa Barbara, Santa Barbara, CA 93106, United States
[b] Materials Science and Technology Division, Los Alamos National Laboratory, Los Alamos, NM 87545, United States
[c] Department of Mechanical Engineering, University of California Santa Barbara, Santa Barbara, CA 93106, United States

ARTICLE INFO

Keywords:
Free surface
Relaxation
Deformation twins
Local stresses
Microscope and HCP metals

ABSTRACT

Deformation twinning is a predominant mode of plastic deformation for hexagonal close packed metals, like Mg and Ti. The heterogenous microstructure and the local stresses associated with twinning play a key role in their mechanical response and fracture. Surface analyses, like electron microscopy, are frequently employed to spatially map microstructure and micromechanical fields in order to study twinning behavior. However, these measurements are inherently influenced by the vicinity of the free surface. Here, an elasto-visco-plastic fast-Fourier-transform (EVP-FFT) polycrystal modeling approach is employed to investigate the effects of free surfaces on twin development before and after loading. We compare calculated micromechanical fields on free surfaces with those calculated inside the bulk and, in some cases, experimental surface measurements. The results indicate that the creation of free surfaces can promote twin propagation and growth and can influence twin morphology by causing a twin lamella to become larger, more blunted and irregular. The structure along the twin boundaries are also affected, due to the higher driving stresses that extend prismatic-basal and basal-prismatic facets. Furthermore, free surfaces invoke different slip activities in the twin and the surrounding parent crystal by enhancing basal, prismatic and pyramidal slip in some localized regions, while reducing slip in others. We demonstrate that the simulated free-surface effects lead to better qualitative and quantitative agreement with experimental measurements from scanning electron microscopy and digital image correlation.

1. Introduction

Deformation twinning in hexagonal close-packed (HCP) crystalline metals, like Mg and Ti and their alloys, is a prevalent mode of plastic deformation due to the scarcity of easy dislocation slip modes. Unlike crystallographic slip, deformation twins develop as 3D subcrystalline domains, which are significantly reoriented from the matrix crystal and impose a finite amount of shear. $\{10\bar{1}2\}$ tensile twins in Mg and Ti, for instance, reorient the crystal by 86.3° and 86.4° and their characteristic shears are 12.9% and 17.4%°, respectively. Consequently, twin domains can generate heterogeneous internal stress within a crystal that can affect strain hardening, overall mechanical response, and trigger damage [1]. Thus, understanding the changes induced in the microstructure and micromechanical fields by twinning is important for establishing the structure-property relationship of HCP metals that twin.

A variety of experimental techniques, including neutron diffraction, X-ray diffraction, and scanning (SEM) and transmission electron microscopy (TEM) in conjunction with digital image correlation (DIC) have been employed to understand the effect twins have on the evolution of internal stresses [2–7]. X-rays allow for non-destructive investigation of the internal microstructure, however, it can be limited in its spatial resolution and interaction volume [8,9]. Electron microscopy techniques offer higher resolution, faster data acquisition, and can collect data over larger areas of the specimen; however, the sample preparation required for these techniques introduces free surfaces near the areas of interest. [9] Due to the nature of the electron microscopy techniques, the interaction volume of the electrons and the sample surface are bounded due to the limited penetration depths of the electrons, often less than 100 μm for SEM and less than 1 μm for TEM. [9] For this reason, sample preparation requires the removal of sections of the material until the region of interest is within 100 μm of the free surface for SEM or the creation of thin films with a thicknesses below 1 μm from the bulk sample for TEM. In both cases, the sample preparation process introduces one or two free surfaces near the region of interest for SEM or TEM, respectively.

The regions of a sample adjacent to free surfaces are physically less constrained than the regions within the bulk, thus prompting unique material behavior. A few works have studied the influence of free surfaces on dislocations and the overall mechanical strength and ductility. For example, Greer et al. suggested a “starvation model” that explains, for thin samples, that the rate of dislocation loss at the free surface can exceed the dislocation multiplication rate, resulting in a limited amount of dislocations available to carry out plastic deformation, consequently

* Corresponding author.
E-mail address: brandonleu@ucsb.edu (B. Leu).

https://doi.org/10.1016/j.mtla.2021.101124
Received 11 January 2021; Accepted 15 May 2021
Available online 20 May 2021

hardening the material [10–12]. Others have described a "truncation model", whereby the truncation of Frank-Read sources by the free surfaces lead to single-ended dislocation sources with shorter dislocations line lengths that increase flow stress [2,13,14]. Experimental TEM evidence has indicated that the escape of dislocations through free surfaces can result in stress, strain and dislocation density gradients between the bulk and surface of the sample [15–17]. The global response of the specimen can be dominated by the surface regions when the sample dimensions are reduced. These results are supported by computational finite element method (FEM) analysis [18]. Furthermore, TEM has shown that free surfaces can directly influence the distribution of dislocation pile-ups near the free surface, which could consequently influence plastic response of the material when compared to the bulk [19].

Computational efforts have also been made to describe the effects of free surfaces on dislocation behavior. Atomistic studies have shown that, in thin samples, the image forces on dislocations near free surfaces are different and can cause the Peierls stresses for dislocation motion to be lower and dislocation mobility to be higher than in the bulk [20–24]. Similar conclusions have been drawn using molecular dynamics (MD) based methods [25,26]. Molecular dynamics simulations have also shown that the stress required for dislocation nucleation near free surfaces are lower than the bulk [27]. Dislocation dynamics simulations have also been implemented in order to capture image force effects on near-surface dislocations that assist in their fast ejection from the surface [28,29]. Crone et al. explained that voids, another source of free surfaces, in Al provided weaker strengthening effects than predicted by classical calculations of Lothe due to long-range image forces that act on the entire dislocation further away from the free surface [30,31].

While free surface effects on dislocation behavior has been a topic of research for some time, the same treatment of free surfaces effects has not yet been extended to deformation twinning. One study by Datta et al., using first-principles, found that twins in Ni are harder to nucleate in thin films than the bulk due to the localization of the electronic structure near free surfaces [32]. Unlike dislocations, the dimensions of twins can be grain-scale, which can result in extensive long-range changes in the local stress states [33]. Any effect of surfaces on local twin stresses can translate to a change in their propagation and growth. The experimentally measured stresses and strains via SEM or TEM could be significantly different when compared to the interior of the bulk sample. Thus, the observations and analysis derived from near free surface techniques on lab scale samples may not directly translatable to the bulk.

In this work, we employ a mesoscale crystal plasticity-based model to quantify free-surface effects and identify those specific regions around the twin that may be the most affected and can influence further twin development. We show that free surface relaxations tend to enhance the stresses along the twin boundary and ahead of the twin tip that would support propagation and growth under applied deformation. The results also find that additional slip modes are activated as a result of the free surface. Comparison with measurements of twin stresses in Ti demonstrates the substantial effect of free surface on in-plane stress fields. These findings can help in bridging properties between lab-scale samples and their bulk counterparts, and potentially reconcile differences between modeling predictions and experimentally measured twin characteristics, such as stress and volume fraction.

2. Computational method

2.1. EVP-FFT formulation for twinning simulation

To study the effects that free surfaces on local stress fields associated with deformation twins, we build upon a crystal-plasticity based elasto-viscoplastic fast-Fourier-transform (EVP-FFT) model [33–35]. It provides a mesoscale modeling framework, capturing the submicron-scale spatially resolved micromechanical fields. EVP-FFT has been used, for instance, to study the development of local stresses and effective mechanical response of heterogenous polycrystalline materials with spatial variations in crystallographic orientation, and elastic and plastic properties [35–37]. More recently, it has been adapted to study deformation twinning in single-crystals, a polycrystal with differing crystallographic orientation and size, parallel twin formation and twin transmission across grain boundaries [33,38–41]. The twin is explicitly formed in a predetermined region by imposing a crystallographic reorientation, according to its twin orientation relationship with the parent crystal, followed by a local transformation shear equal to the characteristic twin shear of the material. Here, we extend the twin modeling EVP-FFT framework to simulate microstructures exposed to a free surface effect.

The model builds upon continuum mechanics principles of equilibrium, kinematic laws and constitutive relationships under an infinitesimal strain approximation. The simulation cell consists of voxels in three dimensions that collectively represent the microstructure. The stress field at every material point x, or voxel, is expressed using Hooke's law as:

$$\boldsymbol{\sigma}^{t+\Delta t}(\boldsymbol{x}) = \boldsymbol{C}(\boldsymbol{x}) : \boldsymbol{\varepsilon}^{e,t+\Delta t}(\boldsymbol{x}) \tag{1}$$

Here, the superscript $t + \Delta t$ denotes time, which is incremented by Δt from time t. In the above equation, $\boldsymbol{\sigma}(\boldsymbol{x})$ is the Cauchy stress tensor, $\mathbf{C}(\mathbf{x})$ is the elastic stiffness tensor, and $\boldsymbol{\varepsilon}^e$ is the elastic strain tensor, which is given by the difference between the total strain tensor, $\boldsymbol{\varepsilon}$, and the plastic strain tensor, $\boldsymbol{\varepsilon}^p$, and the twin transformation strain, $\boldsymbol{\varepsilon}^{tw}$. By following an Euler implicit time discretization scheme, the elastic strain tensor at $t + \Delta t$ can be written as,

$$\boldsymbol{\varepsilon}^{e,t+\Delta t}(\boldsymbol{x}) = \boldsymbol{\varepsilon}^{t+\Delta t}(\boldsymbol{x}) - \boldsymbol{\varepsilon}^{p,t}(\boldsymbol{x}) - \dot{\boldsymbol{\varepsilon}}^{p,t+\Delta t}(\boldsymbol{x})\boldsymbol{\Delta t} - \boldsymbol{\varepsilon}^{tw,t}(\boldsymbol{x}) - \boldsymbol{\Delta\varepsilon}^{tw}(\boldsymbol{x}) \tag{2}$$

The plastic strain and plastic strain rates are constitutively related to the Cauchy stress at every material point x. In this work, visco-plastic deformation is assumed to be accommodated by only dislocation slip on crystallographic slip systems and is expressed as:

$$\dot{\boldsymbol{\varepsilon}}^p = \sum_{s=1}^{N} \boldsymbol{m}^s(\boldsymbol{x})\dot{\boldsymbol{\gamma}}^s(\boldsymbol{x}) = \dot{\boldsymbol{\gamma}}_o(\boldsymbol{x}) \sum_{s=1}^{N} \boldsymbol{m}^s(\boldsymbol{x}) \left(\frac{|\boldsymbol{m}^s(\boldsymbol{x}) : \boldsymbol{\sigma}(\boldsymbol{x})|}{\boldsymbol{\tau}_c^s(\boldsymbol{x})} \right)^{\boldsymbol{n}} \boldsymbol{sgn}\left(\boldsymbol{m}^s(\boldsymbol{x}) : \boldsymbol{\sigma}(\boldsymbol{x})\right) \tag{3}$$

where $\boldsymbol{\tau}_c^s(\boldsymbol{x})$ is the critical resolve shear stress (CRSS) associated with the slip system s, $\dot{\gamma}_o$ is a reference slip rate on the order of the applied rate, and n is the stress exponent (inverse of the rate-sensitivity exponent). The tensor $\boldsymbol{m} = \frac{1}{2}(\boldsymbol{b}^s \otimes \boldsymbol{n}^s)$ is the symmetric part of the Schmid tensor, and b^s and n^s are the unit vectors along the slip direction and normal to the slip plane, respectively, of slip system s.

In the model, twinning is performed explicitly and not considered as an independent pseudo-slip mode. Within the predefined twin domain, during the build-up of twins, the twinning shear increment, γ^{tw}, is explicitly incremented over N^{tw} steps until the characteristic twinning shear, g^{tw}, is achieved on the twin plane and in the twin shear direction of the selected twin variant. The $\boldsymbol{\varepsilon}^{tw}$ and $\Delta\varepsilon^{tw}$ everywhere outside of the twin domain are zero. The increment in the twin transformation strain is written as,

$$\Delta\boldsymbol{\varepsilon}^{tw} = \boldsymbol{m}^{tw}\Delta\boldsymbol{\gamma}^{tw}(\boldsymbol{x}) = \boldsymbol{m}^{tw}\frac{\boldsymbol{g}^{tw}}{\boldsymbol{N}^{tw}} \tag{4}$$

In simulation, $\Delta t = 10^{-4}$s and $N^{tw} = 2000$ is kept sufficiently large to ensure convergence.

2.2. Creation of free surfaces

In the EVP-FFT framework, virtual free-surface formation is simulated in two steps, closely mimicking the sample preparation process. First, the imposed macroscopic load is lifted from the deformed unit cell. Then, a region of virtual material is "removed" via relaxation under zero macroscopic stress until an equilibrium state is reached. The former enforces the unloaded state of the specimen and is achieved in the EVP-FFT simulation by maintaining zero macroscopic stress. The material removal via relaxation is accomplished by reducing the elastic

stiffness in the removed region of unit cell towards zero, which approximates the response of a pseudo-vacuum. While the periodic boundary conditions are enforced, the presence of this pseudo-vacuum region mechanically disconnects each unit cell from its periodic repetitions in the free surface normal direction. By decreasing the elastic stiffness, the material becomes super compliant and the related stresses decrease rapidly. In turn, these stresses affect the plastic strain in the remaining material and new micromechanical fields are recalculated until a new energetic equilibrium is reached. The simulation cell is re-equilibrated over five steps, during which the free surface normal stresses are relaxed to zero. There are no appreciable differences in the micromechanical fields with additional relaxation steps past five steps.

Using this method for free surface creation and relaxation, we study their effects in a situation that represents either an SEM or TEM analysis. In the SEM case, a 2D plane of interest is selected from the center of the bulk simulation cell. All material on one side of the 2D plane are then removed, as described above, to introduce a free surface. The calculated values along the newly created free surface are considered to be affected by the free surface, like those measured experimentally. These predicted free-surface fields only pertain to a thin volume of material near the free surface, as regions far away from the free surface are expected to experience different fields. Accordingly, the values along the same 2D plane within the bulk material, before the free surface creation, represent the bulk response of the material. Similarly, in the TEM case, a thin sheet of material (three voxels thick) is selected from the center of the 3D simulation cell. All materials above and below the thin sheet are removed, introducing two free surfaces. The calculated fields represent free-surface fields, while those generated in the same 2D plane before material was removed are referred to as bulk fields. In contrast with SEM samples, the predicted free-surface fields pertain to the entire TEM sample, since the foil is sufficiently thin such that there are no appreciable gradients in the micro-mechanical fields in the through-thickness direction.

2.3. Materials

The model only requires two sets of material parameters, the elastic constants and CRSS values for the allowed slip modes. Two materials, pure Mg and commercially pure Ti (grade II), are considered in the calculations that follow. The elastic constants C_{11}, C_{12}, C_{13}, C_{33} and C_{44}, of Mg are 59.75, 23.24, 21.7, 61.7 and 16.39 GPa, respectively [42]. The prismatic $\langle a \rangle$, basal $\langle a \rangle$ and pyramidal $\langle c+a \rangle$ slip modes are made available with constant CRSS of 35.7, 3.3, and 86.2 MPa, respectively [43]. Strain hardening is not considered and, therefore, the CRSS values remain constant throughout the simulation. For Ti, the elastic constants C_{11}, C_{12}, C_{13}, C_{33}, and C_{44} are 162.4, 92.0, 69.0, 180.7 and 46.7 GPa, respectively [42]. The CRSS values for the prismatic $\langle a \rangle$, basal $\langle a \rangle$ and pyramidal $\langle c+a \rangle$ slip modes are 90.5, 170.0 and 210.0 MPa, respectively [44].

3. Results

We first consider a model twin microstructure and examine the changes induced by free surface creation on the micromechanical fields around a twin in two different scenarios: after unloading from the deformed state that induced the original twin and after additional external loading. In both cases, we compare fields from within the bulk and in a TEM film.

3.1. Twin formation inside a bulk grain

Fig. 1a shows the 3D model simulation cell containing one $\{10\bar{1}2\}$ tensile twin (in red) embedded in a Mg grain (in gray). A buffer layer surrounding the cell is used to represent the response of the surrounding polycrystalline material. Periodic boundary conditions are applied in all directions. The cell size is $174 \times 174 \times 174$ voxels and the buffer layer is 24 voxels thick, sufficiently large to minimize effects of overlapping fields from periodic images. The orientation of the grain, in Bunge convention, is (0°, 46.7°, 0°) orienting the c-axis of the parent crystal aligned at a 46.7° angle counter-clockwise away from the +*Z*-direction in the YZ plane, as shown in the hexagonal inset in Fig. 1d. Following the twin/matrix orientation relationship, the $(01\bar{1}2)$ twin variant is oriented with its twin-plane normal parallel with the *Z*-direction and the $[0\bar{1}11]$ twin-shear direction along the Y-direction.

The grain without the twin is first subjected to a shear strain of 0.2% in the YZ-direction, resulting in a twin-plane resolved shear stress (TRSS) of about 38 MPa. To form the twin, the predetermined twin domain is reoriented according to its twinning relationship with the parent matrix orientation, while under the applied strain. The geometry of the twin resembles an oblate spheroid with a minor axis of 15 voxels and a major axis of 60 voxels long. A characteristic twin shear of 12.9% is then slowly incremented on the twin plane in the twin shear direction in order to form the twin over 2000 steps. In each step, the strain and stress tensor fields are calculated everywhere in the simulation cell using the EVP-FFT formulation presented in Section 2.1.

3.2. Stress relaxation during free surface formation

We compare the stress fields on a 2D plane of interest within the bulk of the material and from the same plane taken along the free surface. A small region centered around the twin tip, outlined in white dashed lines in Fig. 1b and c, is taken for inspection; this subsection is truncated on the left side at the center of the twin. In Fig. 2, the left column shows the stress fields in the bulk, the middle column shows those on the free surface, and the right column shows the difference between the two. The twin boundary is outlined in black for clarity.

The top row, Fig. 2a–c, shows the normal stress out-of-plane in the X-direction, σ_{xx}. The second row, Fig. 2d–f, and third row, Fig. 2g–i, show the in-plane normal stress components in the Y-direction and Z-direction, σ_{yy} and σ_{zz}, respectively. The positive regions, in red, indicate a tensile stress, while the negative regions, in blue, represent compressive stresses. Inside the twinned region in the bulk, σ_{xx} is compressive (Fig. 2a), while σ_{yy} is near zero (Fig. 2d) and σ_{zz} is tensile (Fig. 2g). Both above and below the center of the twin, the stresses are tensile. The regions above the twin tip are tensile, while below the twin tip they are mostly compressive. Along the free surface, the σ_{xx} field is uniformly zero everywhere (Fig. 2b), as expected for a free surface. The other two shear stress components, σ_{xy} and σ_{xz}, are also uniformly zero, as expected, but not shown in the interest of space. In the free surface sample, we find that the σ_{yy} and σ_{zz} fields are nearly identical (Fig. 2e and h), and compared to the same fields in bulk, the intensity of these stresses has reduced (Fig. 2d and g).

3.3. TRSS fields in the bulk vs at the free surface

Fig. 2j and k show the twin plane resolved shear stress, τ_{TRSS}, fields around a twin lying in the bulk and at the free surface, respectively. Both fields are heterogeneous in stark contrast to the homogeneous τ_{TRSS} field of ~38 MPa across the crystal before the twin was formed. In the case of the bulk twin, the τ_{TRSS} in regions inside and immediately surrounding the twin are negative, meaning that they act in the anti-twinning sense. The drop in stress from 38 MPa before twinning to the severe anti-twinning values (e.g., −85 MPa) signifies a strong "back-stress" [34,39,45]. When generated along the twin boundary, this back-stress restricts thickening of the twin or growth normal to the twin plane. At the same time, a positive τ_{TRSS}, ~60 MPa, develops in the crystal in front of the twin and is the strongest directly at the twin tip. This "forward stress" drives the twin tip to propagate. These results agree well with previously reported works [33,40,41,46].

The τ_{TRSS} field in the thin film for the same 2D plane shows many interesting differences compared to those in the bulk. As seen in Fig. 2l, the TRSS fields in the thin film have increased everywhere compared to

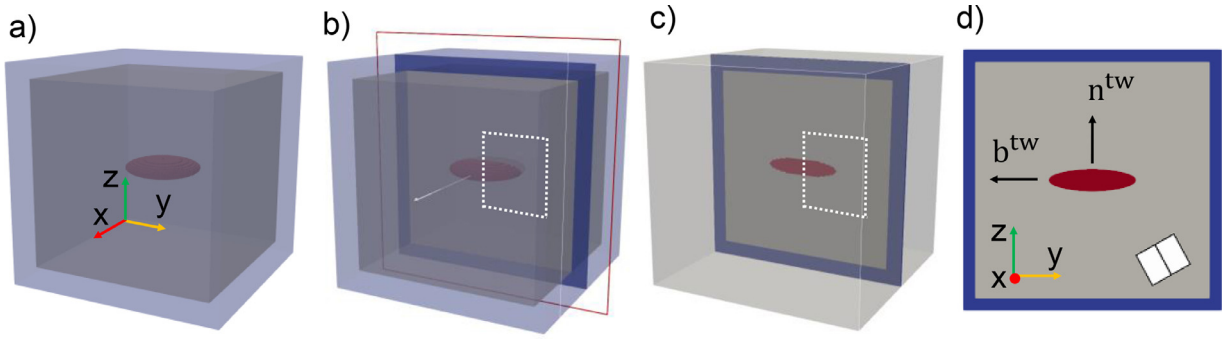

Fig. 1. Schematic representation of an oblate spheroid twin embedded in a Mg grain. (a) The ellipsoidal twin (red) is formed in a parent matrix grain (gray). The parent matrix is surrounded by a homogeneous layer (blue) with uniformly distributed crystal orientations that approximates a polycrystalline medium. (b) The red outline highlights the 2D slice, parallel to the *Y-Z* plane, taken from the center of the simulation cell. The values on this slice represent the bulk material response. (c) A thin film is formed by taking a central section out of the 3D simulation. The layers in front and behind the thin film are "removed" by setting their elastic properties to be super compliant. (d) A 2D view down the center of the twin. 2D slices can be taken from either the bulk (from Fig. 1b) or at a free surface (from Fig. 1c). The crystallographic orientation of the parent matrix is shown in the hexagonal inset (For interpretation of the references to color in this figure legend, the reader is referred to the web version of this article.).

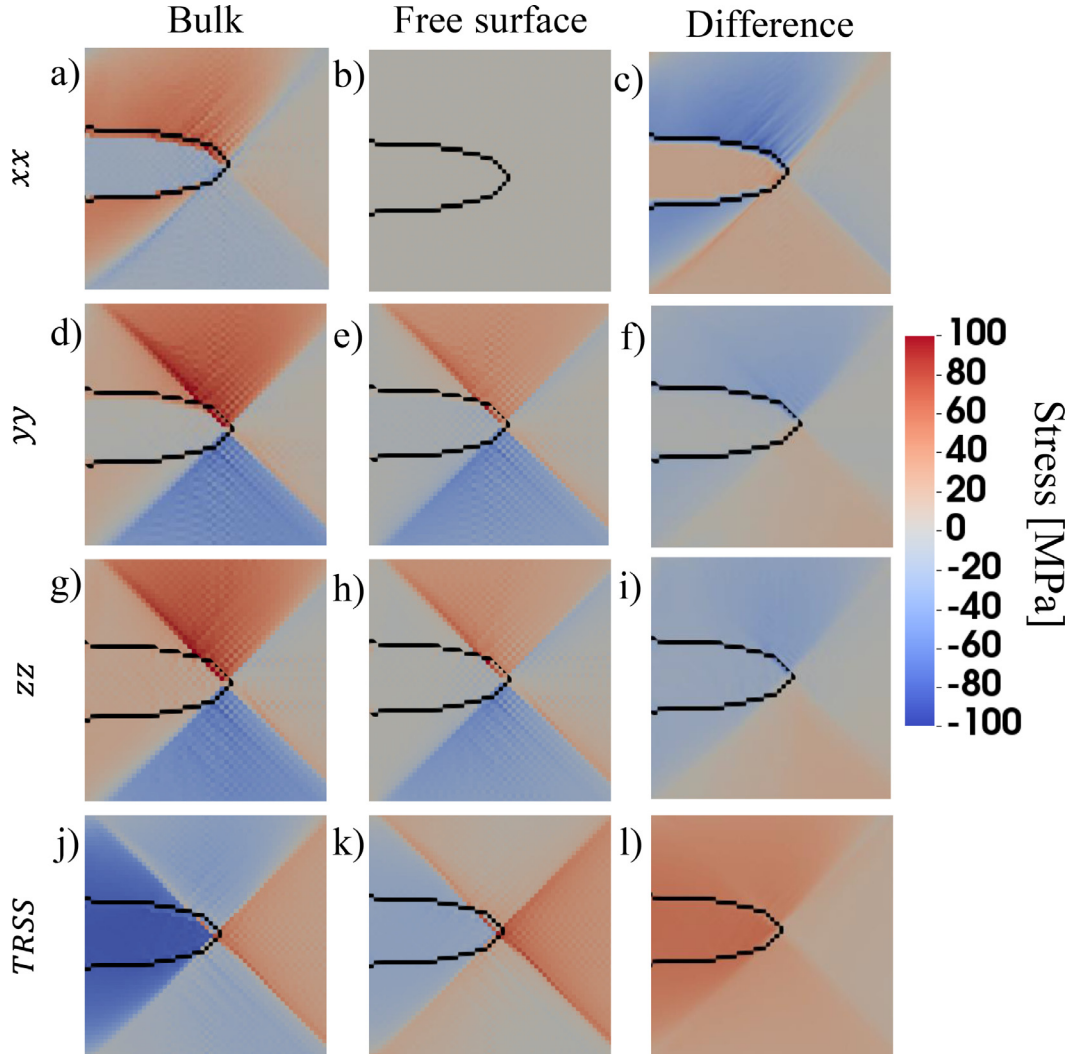

Fig. 2. Comparison of the simulated σ_{xx}, σ_{yy}, σ_{zz} and τ_{TRSS} stress field distribution found within the bulk (left column) and within the thin film (middle column). The right column shows the difference in stress levels between the bulk and the thin film. (a–c) corresponds to σ_{xx}. (d–f) corresponds to σ_{yy}. (g–i) corresponds to σ_{zz}. (j-l) corresponds to τ_{TRSS} (For interpretation of the references to color in this figure, the reader is referred to the web version of this article.).

the bulk, in ways that generally support twin tip propagation and thickening. Notably, the strong forward stress concentration directly in front of the twin increases to 70 MPa from ~60 MPa, and the regions above and below the twin tip that were previously negative (anti-twinning) in the bulk have become positive (for twinning). Inside the twin domain and near the twin boundaries, where the values of the backstress were the most severe, the TRSS fields have increased to about −30 MPa, reaching values almost three times higher in thin film than that in the bulk.

3.4. Plastic accommodation in the bulk and at the free surface

The stresses generated both inside and outside the twin region are sufficient to locally activate slip. In the case of the twin in the bulk, Fig. 3a–c identifies the total shear strain from each slip mode in Mg: basal $\langle a \rangle$, prismatic $\langle a \rangle$, and pyramidal-I $\langle c + a \rangle$ slip modes. Generally, basal slip in the surrounding parent matrix accommodates most of local deformation imposed by the twin. Relatively large amounts of basal slip accumulate in regions that radiate diagonally from the twin tip (Fig. 3a), while prismatic slip is limited (Fig. 3b) and pyramidal-I slip is only activated inside the twin region (Fig. 3c).

To identify the types of dislocations that would be promoted ahead of the (stationary) twin under further loading and/or twin development, Fig. 3d–f presents the fields of maximum absolute resolved shear stress (RSS) among the slip systems belonging to each slip mode. The maximum RSS serves to indicate the slip system most likely to activate, however, not the only system that could be activated. It can be seen in Fig. 3d that the driving stress for basal slip is highly concentrated in regions that lie diagonally from the twin tip and are close to the CRSS of 3.3 MPa, suggesting basal activation is likely. Basal slip is not likely, however, in the twin domain, where the driving stress is almost zero. The RSS field for prismatic slip in Fig. 3e is split into two regions separated by a diagonal centered at the twin tip. In neither regime is prismatic slip likely. The stresses in the upper left region reach ~21 MPa and within the twin are ~25 MPa, both below the CRSS of 35.7 MPa. The RSS field for pyramidal-I slip is moderately high within the twin, in the matrix near the twin boundary, and concentrated at the twin tip, as seen in Fig. 3f; however, they are still well below the CRSS of 86.2 MPa, indicating that they are not likely to be activated. According to this analysis, basal slip was the only slip mode that the twin stress fields promote in the bulk.

Starting with the twin in the bulk, the creation of free surfaces is simulated by relaxing the stresses in the out-of-plane directions to zero to mimic the conditions of a thin film. Fig. 3g–i presents the total plastic accommodation by each slip mode of the microstructure that occurred *only* from the introduction of the free surfaces. As seen in Fig. 3g, the free surface creation develops concentrated regions of basal slip activity that lie diagonal from the twin tip. Similarly, plastic strain accumulated by prismatic slip in a region extending diagonally across the twin tip, moving from the bottom-left to top-right, see Fig. 3h, although to a much lesser degree than basal slip. A little plastic strain by pyramidal slip is predicted to accumulate in a concentrated region just at the twin tip, Fig. 3i.

In contrast to bulk RSS fields (Fig. 3d–f), j–l show the maximum absolute RSS distributions in the thin film for the most stressed basal, prismatic, and pyramidal-I slip systems. These RSS fields help to identify the slip activity promoted by twinning in the thin film. Similarly to the bulk case (Fig. 3d), in the thin film (Fig. 3j) the maximum RSS for basal slip is strongly concentrated in fine regions emanating diagonally from the twin tip, with values at the CRSS of 3.3 MPa. Additionally, moderately high levels of RSS develop in the parent matrix but little driving stress for basal slip develop within the twin region itself. The prismatic RSS fields for the thin film (Fig. 3k) have completely reversed from those in the bulk (Fig. 3e). The driving stresses in the upper left region, that were previously high in the bulk, have been reduced while the regions in the bottom right, that were previously low, have been enhanced. In Fig. 3k, the RSS almost reaches the CRSS, suggesting prismatic slip activity in a concentrated region radiating diagonally from the twin tip. Lastly, Fig. 3l shows the maximum RSS distribution for pyramidal slip in the thin film. In the bulk (Fig. 3f) the regions of maximum pyramidal RSS that were previously highest were inside twin domain. In contrast, in the thin film (Fig. 3l) the pyramidal RSS values in the twin are relatively low, around 25 MPa. At the same time, the stress concentration at the twin tip in the parent crystal has increased to about 65 MPa. However, it is still not sufficient to activate pyramidal slip. Thus, in the thin film, both prismatic slip and basal slip are activated ahead of the twin, unlike in the bulk, where only basal slip was activated.

3.5. Twin thickening in the bulk versus thin film

Next, we investigate the difference in the propensity for twin propagation and growth between the twin in the bulk and in the thin film under additional externally applied load. In simulation, the same shear is applied to both the bulk sample, Fig. 1b, and the thin film sample, Fig. 1c. Fig. 4 compares the TRSS fields that develop from deforming the bulk sample with those from deforming the thin film. In both cases, an external shear of 0.2% is applied along the *Y*-direction (parallel to twinning shear) in the *Z*-plane (parallel to the twinning plane). The two fields show many differences. In the bulk, the TRSS is negative inside the twin matrix and along the lateral regions of the twin just outside the twin boundary in the parent matrix, with values of about −34 MPa. At the same time, the TRSS in the thin film is positive everywhere inside the twin and the surrounding parent matrix, with values of about 40 MPa. In the bulk, the values were negative for these same regions. In both cases, a cone-shaped stress concentration region develops at the twin tip, reaching values of 70 MPa and 88 MPa for the bulk and thin film cases, respectively. In the bulk case, the regions just above and below the twin tip are near zero, while the same regions in the thin film case reach up to 70 MPa. Thus, the twin loaded in a thin film has a higher propensity to propagate forward and grow thicker than the same twin loaded in bulk.

4. Discussion

4.1. Free surface effects on twin morphology

The calculated TRSS field changes shown in Fig. 2l indicate that the local driving forces for twin development are altered by the free surface. Under the same continued loading, a twin in the bulk could, therefore, grow and adopt a different morphology than the same twin observed in the thin film. In the bulk, in Fig. 2j, the twin domain and the parent matrix near and along the twin boundaries experience large back stresses, resisting twin thickening normal to the twin plane. The region in front of the twin, however, is highly positively stressed, promoting lengthwise twin tip propagation. In contrast, in the thin film, as depicted in Fig. 2k, the regions inside the twin and along the twin boundaries experiences less anti-twinning stress. The backstresses in these regions are up to three times weaker in the thin film than in the bulk, providing less resistance to twin thickening. Consequently, twins in the bulk should have higher aspect ratios (i.e., thinner twins) than twins near free surfaces.

Reduced backstresses in the lateral regions of the twin imply that thickening of the twin near free surfaces would receive less resistance than inside the bulk, potentially resulting in larger twin volume fractions near the surface under an applied load. This trend is consistent with some experimental observations of twins in AZ31 Mg alloys. The twin volume fraction obtained through near-free surface techniques, such as EBSD in an SEM, on AZ31 deformed to 0.2% strain is approximately 3.5% [47]. In the same material (same alloying and texture) and loading condition, neutron diffraction techniques measured a twin volume fraction more than 50% lower in the interior of an AZ31 alloy deformed to 0.2% strain [48]. While some differences may be expected due to the assumptions these techniques made in extracting twin volume fractions,

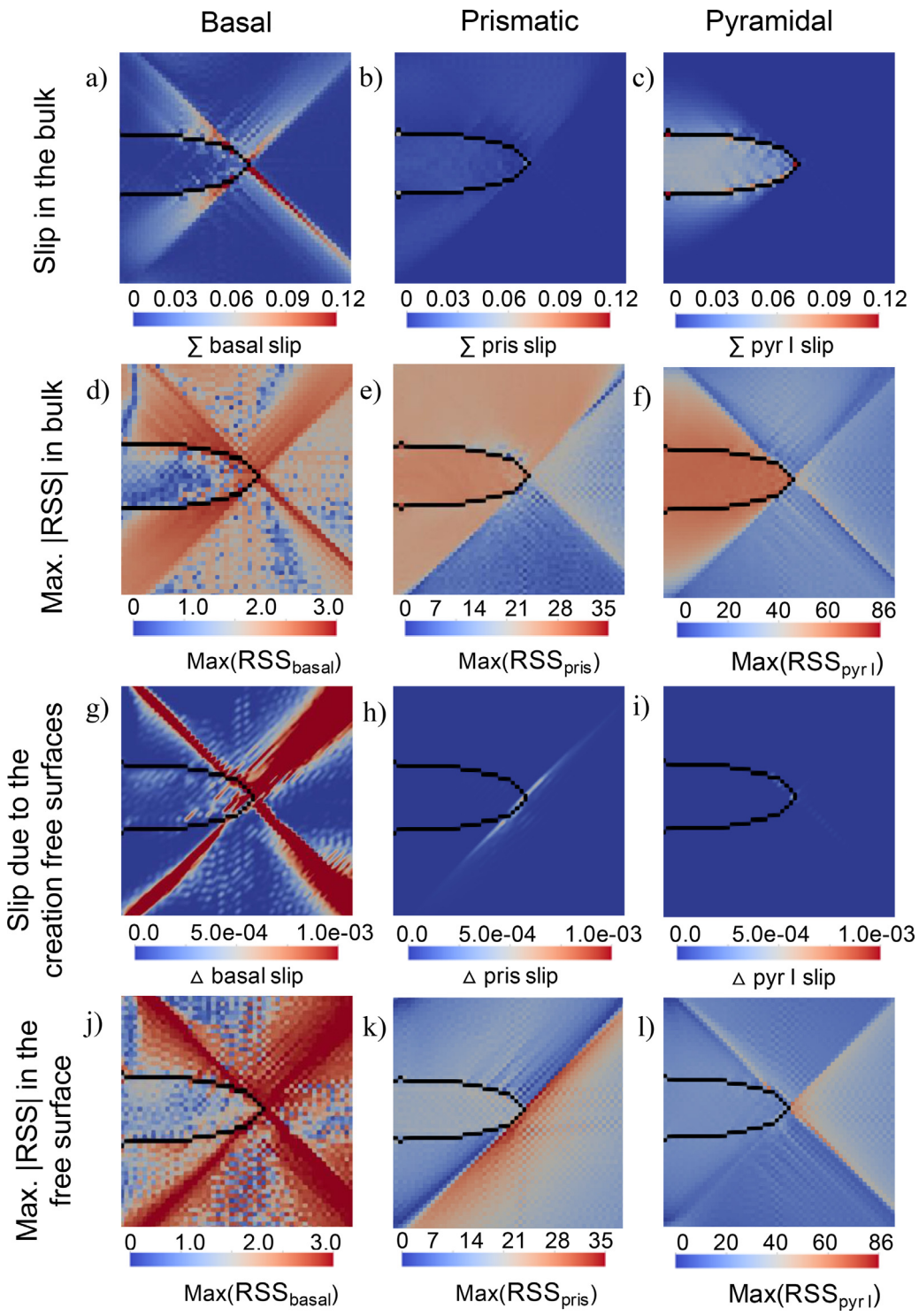

Fig. 3. The total accumulated slip that develops as a result of the initial externally applied load and the formation of the twin. The values represent the sum of the accumulated slip amongst all (a) basal, (b) prismatic, and (c) pyramidal type-I slip systems. The distribution of maximum absolute RSS amongst the (d) basal, (e) prismatic, and (f) pyramidal systems in the bulk. The total plastic slip accumulated only during the free surface relaxation process for (g) basal, (h) prismatic, and (i) pyramidal slip. The distribution of maximum absolute RSS in the (j) basal, (k) prismatic, and (l) pyramidal systems in the free surface.

they cannot explain the substantial drop. Free surface effects could have helped make twin growth easier by increasing the driving force for twinning all around the twin boundary.

Additionally, the analysis suggests that the shape of the twin tip could differ between the bulk twin and the thin film twin. In Fig. 2k for the thin film, we observe that the regions directly above and below the twin tip in thin film have approximately 20 MPa TRSS. In the bulk case, however, the same regions in Fig. 2d, have backstresses of about −35 MPa. The introduction of free surfaces may cause this region to twin, while if it remained in the bulk, this event would be unlikely. In this case, the newly developed positive TRSS immediately surrounding the twin tip could be sufficient to alter the twin morphology, resulting

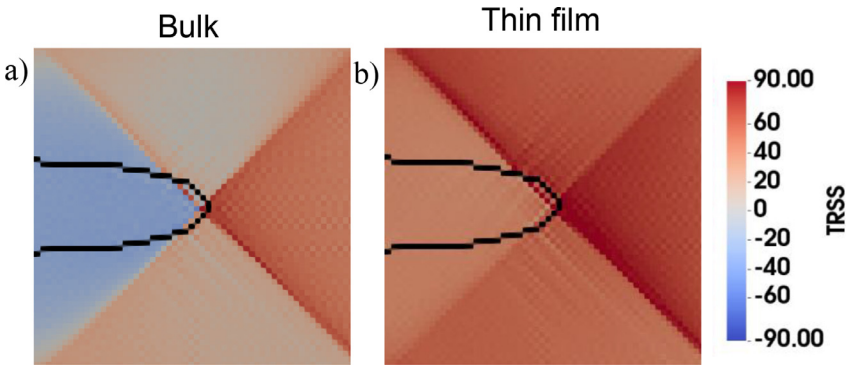

Fig. 4. Comparison of the TRSS fields that develop with additional macroscopic YZ-shear straining applied after the twin has been formed. TRSS fields that develop when deforming the (a) bulk and (b) thin-film virtual samples.

in a severely blunted twin tip in the thin film case when compared the bulk.

4.2. Free surface effects on slip activity

The results in Fig. 3a–c indicate that mainly basal slip accommodates the twin in the matrix while pyramidal slip occurs only in the twin and prismatic slip is limited everywhere. However, as seen in Fig. 3g–i, by introducing free surfaces, basal and prismatic slip can be locally induced. The analysis points to a tendency for surface characterization techniques to overestimate the amount of basal and prismatic slip around twin tips since some amount of dislocations will arise solely due to the free surface relaxation. This is further complicated by the disparity in the maximum RSS among prismatic and pyramidal slip systems in the bulk, Fig. 3e–f, and in the free surface, Fig. 3k–l. In the bulk, Fig. 3e–f, the RSS for prismatic and pyramidal slip are insufficient to activate but are still substantial, within 20% of the CRSS. Under more complex microstructures and loading conditions, the regions with enhanced prismatic and pyramidal RSS may activate. However, these enhanced stresses diminish greatly in the free surface. Instead, other regions become more favorable for prismatic and pyramidal slip, Fig. 3k and 3l, respectively. Recent work by Jiang et al., show both $\langle a \rangle$ and $\langle c + a \rangle$ dislocations are observed at the twin front during in-situ deformation that coincides well with the predicted regions of enhanced RSS on basal, prismatic, and pyramidal slip systems in the thin film, seen in Fig. 3j–l [49]. Observations of plastic accommodation of twins made with near surface techniques may not be translatable to twin/matrix plastic behavior inside the bulk. Evidently, the stress fields around twins are complex and the introduction of free surfaces near twins can dramatically change the stress fields.

4.3. Free surface effects on twin propagation

We next consider the stress fields that develop after additional external load is applied to both the bulk and thin film containing the same twin. Three interesting features indicate different twinning behavior due to the free surface. First, backstresses still persist in the twin and the nearby surrounding parent matrix of the bulk, inhibiting twin growth, seen in Fig. 4a. At the same time, in the thin film, Fig. 4b, the stresses in the same regions show no backstresses, implying that twins near free surfaces can grow thicker with a more blunted twin tip. Secondly, the forward stresses at the twin tip are stronger in the thin film case than the bulk, implying that the driving force for twin propagation is higher as well. Lastly, the TRSS fields that develop in the thin film are not symmetric about the twinning shear direction, unlike the bulk case. In the bulk material, the strongest TRSS concentration occurs at the twin tip; however, in the thin film case, both the twin front and region above the twin tip experience strong stress concentrations.

Deforming the thin film caused the development of inhomogeneous stress distributions around the twin, especially near the twin tip. These local stress concentrations may be enough to initiate twins of different variants to emit from the twin boundary or cause section of the twin front to propagate earlier than others. This might help to explain why many twin embryos are seen to be emitted from twin boundaries during some in-situ deformation studies [49]. Additionally, the heterogenous driving forces may cause the twin tip to propagate asymmetrically about the twinning shear direction upon loading.

4.4. Free surface effect on twin boundary characteristics

Thus far, our analyses of twin growth have been based on the sign and severity of TRSS fields near and along the coherent twin boundaries (CTB) of the lamellae. However, in some parts of the twin, particularly near its tip region, the twin boundary structure can be faceted and comprised of basal-prismatic (BP) or prismatic-basal (PB) boundaries that separate CTBs [50–53]. Unlike the CTBs, the formation and migration of BP and PB boundaries are controlled by the normal stresses acting on these planes. In Mg, the separation of basal and prismatic planes are 5.21 A and 5.55 A , respectively [46]. Thus, to migrate BP or PB boundaries, the normal stresses need to be tensile or compressive, respectively. Fig. 5 illustrates the stresses, σ_{BP} and σ_{PB}, normal to the BP and PB boundaries that drive their mobility, respectively.

TEM observations of PB/BP facets in twin boundaries report facets several nm long [50,51,54–57]. These lengths are significantly greater than predictions by atomistic simulations, where the facets are on the order of 4–6 atoms long [55,56,58–61]. TEM measurements on thin foils are influenced by the free surface, while most atomistic simulations employ periodic boundary conditions that better approximates a bulk response. To determine whether free surface effects can help to explain the observed differences, we calculate the σ_{BP} and σ_{PB} fields taken within a plane in the bulk with that from an identical plane in a thin foil. In Fig. 5, the left column shows the σ_{BP} and σ_{PB} stress fields in the bulk, the middle column shows those on the free surface, and the right column shows the difference between the two. The red regions indicate a positive tensile stress, while the blue regions represent a compressive stress. As seen in Fig. 5a and 5d, in the bulk, σ_{BP} and σ_{PB} along the twin boundary are compressive and tensile, respectively, which is unfavorable for the formation and migration of the facets. After the creation of the free surface, however, σ_{BP} increases by about 40 MPa and σ_{PB} decreases by about 70 MPa, Fig. 5c and 5F, respectively. This suggests that introducing free surfaces can help migrate the facets, consequently leading to longer facets, schematically illustrated in Fig. 5g and h. The more favorable stress conditions near free surfaces can thus help to provide an explanation for the discrepancies between measurement and atomistic simulation calculations of twin facet size.

4.5. Bridging free surface effects between lab-scale observations and bulk response

Additional surface relaxation calculations are performed in comparison with direct experimental measurements of twin stresses across a

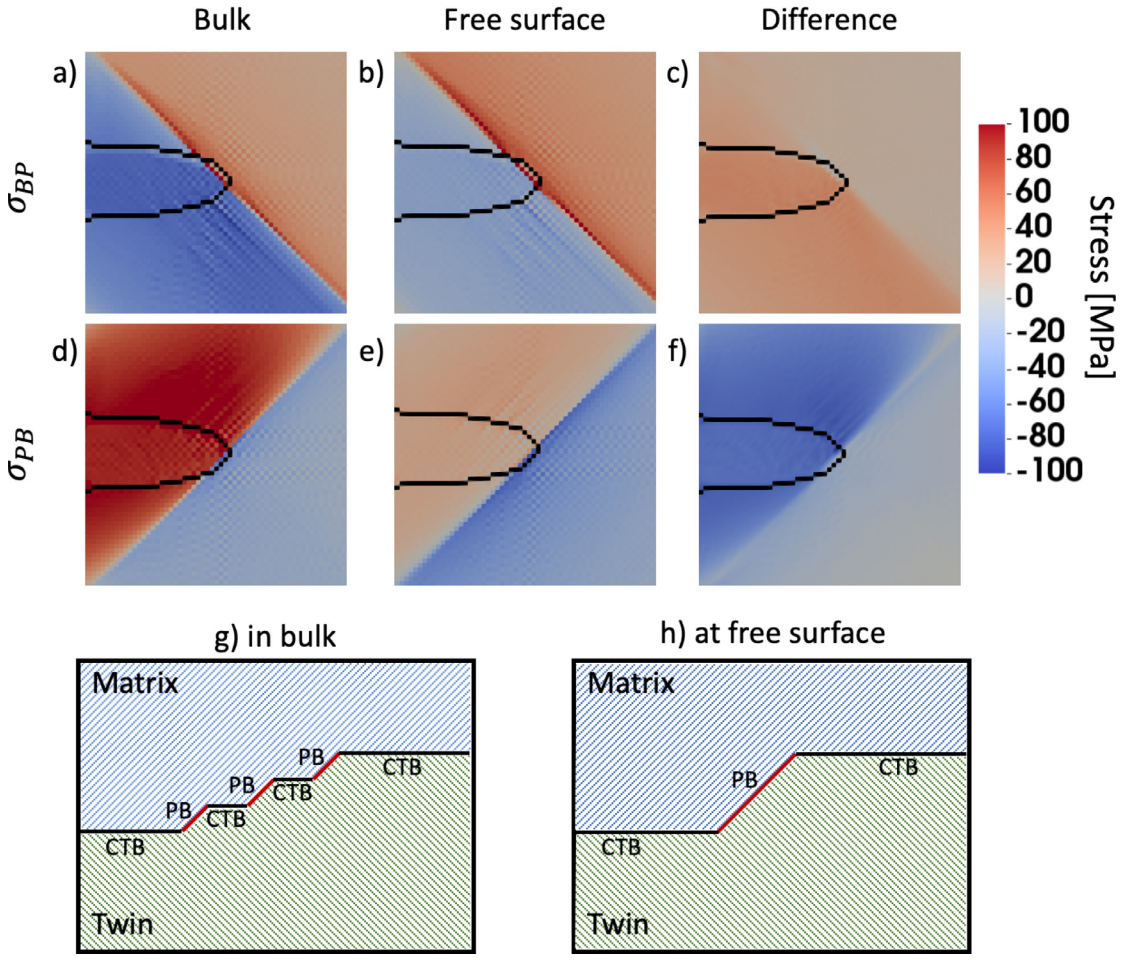

Fig. 5. Distribution of normal stresses to PB and BP facets within the bulk (left column) and within the thin film (middle column). The right column shows the difference in stress levels between the bulk and the thin film. First and second rows correspond to stresses normal to BP and PB facets, respectively. Schematic representation of BP and/or PB facets in the bulk (g) and at the free surface (h) (For interpretation of the references to color in this figure, the reader is referred to the web version of this article.).

grain boundary in Ti [5]. Basu et al. employed a correlative technique using EBSD with DIC on commercial grade II titanium deformed at room temperature in an in-situ four-point-bend test [5]. The surface of the specimen was prepared for EBSD prior to deformation. Using DIC, they mapped the grains in a small region of the microstructure in the twinned polycrystalline Ti sample, shown in the Fig. 6a, taken from the tensile surface of the bent specimen strained to 18%.

This same region is digitized to create a pseudo-3D microstructure, consisting of columnar grains extending in the out-of-plane direction for simulation. The simulation cell size is $5 \times 210 \times 310$ voxels. For the twin in the model, the twin shear direction and twin plane normal lie in-plane as in the experiment [5]. The microstructure was compressed by 18% in the normal direction, out-of-plane. We consider two cases; the first one has a free surface on one side, formed by removing two layers in the out of plane direction, designed to compare directly with the EBSD-DIC measurement, and the second case considers the same twin but, hypothetically, in the bulk far from the free surface. Fig. 6c compares the TRSS fields, taken along the line AB illustrated in the Fig. 6b, crossing from a twinned region to the neighboring grain. The red symbols show the experimentally measured TRSS, the blue dots show the calculated TRSS in the free surface, and the black dots show the calculated bulk TRSS taken from a 2D slice at the center of the whole simulation cell. Compared to the experimentally measured values, the TRSS at the free surface (blue symbols) give a better comparison both qualitatively and quantitatively than those calculated within the bulk (black symbols).

The calculations show that the effect of the free surface is to lower the backstresses and stress concentrations produced in the neighboring grain at the twin/grain boundary junction. At the simulated free surface inside the twin but away from the grain boundary, TRSS levels of about −53 MPa are predicted, in good agreement with experimental observations of about −50 MPa. Calculated values inside the bulk predict TRSS levels of about −100 MPa. Experimentally, the negative TRSS inside the twin decreased moving towards the grain boundary. A small TRSS gradient is predicted along the free surface case, while almost no TRSS gradient arises within the bulk simulation. In the neighboring grain, the calculated free surface TRSS reaches a maximum of about 60 MPa and decreases moving away from the grain boundary. This decay is also in good agreement with experimental observation, where the maximum TRSS is about 50 MPa and decreases moving away from the grain boundary. Similar trends were observed in the bulk of the simulation, however, with a higher maximum of ~90 MPa and a larger gradient. The results in Fig. 6 help to validate the effectiveness of taking into account free surface effects in the accurate representation of simulated materials. Furthermore, this approach offers a way to gain insigh that may help to bridge a connection between the results obtained from lab-scale samples and what can be expected in their bulk counterparts.

While overall good agreement is achieved when free surfaces are modeled, some quantitative differences are noted. The calculated near grain boundary stresses deviate slightly in value, a difference that can be attributed to the fact that the actual grain boundaries are much more

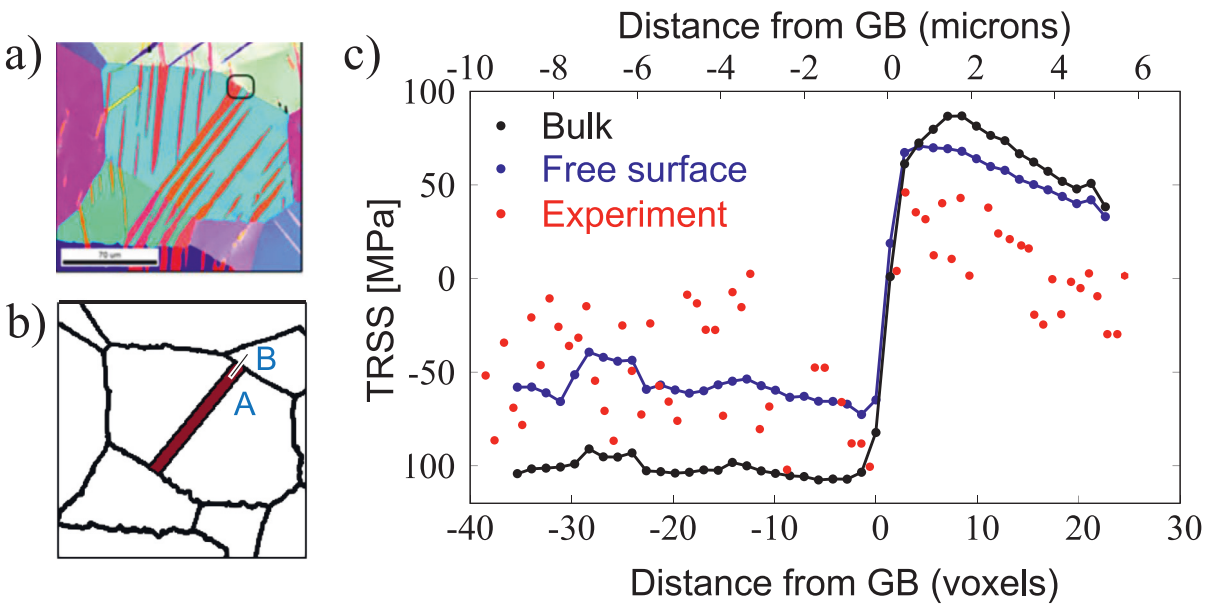

Fig. 6. Comparison between the calculated and measured TRSS fields across a grain boundary in polycrystalline Ti. a) EBSD image of the region of interest taken from Basu et al. [5] with the twin tip and grain boundary circled in black. b) Shows the digitized microstructure used for the EVP-FFT simulation. Only one twin is simulated in order to isolate the stress fields produced from the twin. c) Comparison between calculated TRSS levels in the bulk (black) and at the simulated free surface (blue) and the experimentally measure values (red) measured along line AB seen in Fig. 6b (For interpretation of the references to color in this figure legend, the reader is referred to the web version of this article.).

complex and more morphologically rough than those represented in the model. The overlapping fields from nearby twins seen in EBSD were not included in the simulation and it is possible that these are non-negligible [40]. The modeling method introduces a perfectly flat free surface, one that does not account for any surface damage effects commonly associated with sample preparation, such as mechanical polishing, electrochemical polishing or ion beam milling and are highly dependent on the material itself [9,62]. Both the deformation and sample preparation may have introduced some strain hardening, while, for simplicity, no strain hardening was considered in these calculations. Last, apart from in-plane sources, there is the influence of out-of-plane differences between the sample and model. Without information on the subsurface structure, the present model is quasi-3D columnar and the constraints on the surface grains from those neighbor grains below the sample surface may not be the same.

5. Conclusions

In this study, we employed a full-field crystal-plasticity based elasto-visco-plastic fast-Fourier-transform (EVP-FFT) model to simulate the effects of free surfaces on the stress fields developing in and around a twin. The results help to forecast how these effects may influence slip activity and further twin propagation and growth. In close approximation to TEM sample preparation, a model thin film was sectioned from the center of the simulation cell by removing material on both sides of the film in order to simulate the creation of free surfaces. Material removal was accomplished by setting the materials on both sides the thin film to be elastically isotropic and super compliant, approximating the response of a vacuum.

The model provides for calculations of the micromechanical fields that would develop during different stages typically involved in characterization. First, in the bulk sample after twinning, then in the thin film sample after free surface relaxation. Later, the bulk twinned material and the thin film material containing a twin are independently loaded to study how the twin may continue developing in each. Overall, the results predict different behavior between the bulk and thin film responses. The following conclusions are drawn:

- Free surface relaxation, in general, increases TRSS fields inside and surrounding twin, thus enhancing twin tip propagation and twin thickening. Also, twin tip blunting and asymmetric propagation are promoted near free surfaces relative to the same twin in bulk. Twin volume fractions in the interior of the bulk may be much lower than commonly reported by microscopy observations.
- Under further loading, the results suggest that twins near free surfaces would tend to assume a lower aspect ratio (twin length in shear direction/twin thickness in the normal direction) than in the bulk, resulting in thicker twins with blunted tips.
- Twin boundary structure can be influenced by free surfaces. Basal/prismatic (BP) and prismatic/basal (PB) facets migration are promoted near free surfaces, resulting in longer facets than in the bulk. This may help to reconcile some discrepancies between TEM observations and atomistic simulations.
- The introduction of free surfaces itself is sufficient to activate basal, prismatic and pyramidal slip in localized regions ahead of the twin. That is, basal slip is concentrated in two localized bands emanating diagonally from the twin tip. Prismatic slip is concentrated in a single thin band centered at the twin tip. Pyramidal-I slip is slightly produced at the twin tip.
- The plastic response of the twin matrix and the surrounding parent matrix is different in the bulk when compared to a thin film.
- Basal slip activates more readily in the thin film due to higher driving stresses.
- Prismatic slip is possible inside the twin in the bulk, but less likely in twin in the thin film due to reduced driving stresses from free surface relaxation. Free surface relaxation activates prismatic slip at the twin tip in the thin film that would otherwise not be activated in the bulk.
- Pyramidal slip is imminent inside the twin and the surrounding parent matrix in the bulk, but free surface relaxation reduces the driving stresses, making pyramidal slip in these regions unlikely in the thin

film. At the same time, free surface relaxation enhances the driving force for pyramidal slip at the twin tip when compared to the bulk.

By simulating free surface relaxations, computed micromechanical fields become quantitatively and qualitatively more comparable to experimentally measured values taken from near free surface techniques, such as SEM and TEM. Elucidating the differences in these fields could help in translating experimentally measured values to bulk material behavior. While we focus this study on $\{10\bar{1}2\}$ tensile twinning in Mg and Ti, the findings of this study can be extended to other twinning modes in other material systems, since micromechanical fields originate from the twin reorientation and shear that is intrinsic among all twins, although to varying degrees.

Declaration of Competing Interest

None.

CRediT authorship contribution statement

B. Leu: Conceptualization, Methodology, Formal analysis, Investigation, Visualization, Data curtion, Writing – original draft, Funding acquisition. **M. Arul Kumar:** Conceptualization, Methodology, Resources, Supervision, Writing – review & editing, Funding acquisition. **I.J. Beyerlein:** Conceptualization, Resources, Supervision, Writing – review & editing, Funding acquisition.

Acknowledgments

B. L. was supported by the Department of Defense (DoD) through the National Defense Science & Engineering Graduate Fellowship (NDSEG) Program. M.A.K. acknowledges the financial support from the U.S. Department of Energy, Office of Basic Energy Sciences (OBES) FWP-06SCPE401. I.J.B. acknowledges financial support from the National Science Foundation (NSF CMMI-1728224).

References

[1] M. Knezevic, M.R. Daymond, I.J. Beyerlein, Modeling discrete twin lamellae in a microstructural framework, Scr. Mater. 121 (2016) 84.
[2] P. Rangaswamy, et al., Metallurgical and Materials Transactions A: Physical Metallurgy and Materials Science 33a (2002) 757.
[3] O. Muránsky, D.G. Carr, P. Šittner, E.C. Oliver, Int. J. Plast. 25 (2009) 1107.
[4] H. Abdolvand, M.R. Daymond, Acta Mater. 60 (2012) 2240.
[5] I. Basu, H. Fidder, V. Ocelík, J.T.M de Hosson, Crystals 8 (2017) 1.
[6] C.C. Aydiner, J.V. Bernier, B. Clausen, U. Lienert, C.N. Tomé, D.W. Brown, Evolution of stress in individual grains and twins in a magnesium alloy aggregate, Phys. Rev. B 80 (2009) 1.
[7] L. Balogh, et al., Acta Mater. 61 (2013) 3612.
[8] P.J. Withers, P.J. Webster, Strain 37 (2001) 19.
[9] Y. Leng, *Materials characterization: Introduction to microscopic and spectroscopic methods*, Second edition, John Wiley & Sons, 2013.
[10] J.R. Greer, W.D. Nix, Phys. Rev. B Condens. Matter Mater. Phys. 73 (2006) 1.
[11] J.R. Greer, W.C. Oliver, W.D. Nix, Acta Mater. 53 (2005) 1821.
[12] Z.W. Shan, R.K. Mishra, S.A. Syed Asif, O.L. Warren, A.M. Minor, Nat. Mater. 7 (2008) 115.
[13] J. Senger, D. Weygand, P. Gumbsch, O. Kraft, Scr. Mater. 58 (2008) 587.
[14] H. Tang, K.W. Schwarz, H.D. Espinosa, Acta Mater. 55 (2007) 1607.
[15] H. Suzuki, S. Ikeda, S. Takeuchi, J. Phys. Soc. Japan 11 (1956) 382.
[16] J.T. Fourie, Philos. Mag. 17 (1968) 735.
[17] H. Mughrabi, Phys. Status Solidi 44 (1971) 391.
[18] C. Keller, E. Hug, A.M. Habraken, L. Duchene, Int. J. Plast. 29 (2012) 155.
[19] F. Pettinari-Sturmel, G. Saada, J. Douin, A. Coujou, N. Clément, Mater. Sci. Eng. A 109 (2004) 387–389.
[20] L. Liu, Z. Meng, G. Xu, C. He, X. Wu, R. Wang, Adv. Mater. Sci. Eng. (2017) 2017.
[21] B. Gars, X. Markenscoff, Philos. Mag. 92 (2012) 1390.
[22] W. Wu, R. Schäublin, J. Chen, J. Appl. Phys. (2012) 112.
[23] C.L. Lee, S. Li, Acta Mater. 55 (2007) 2149.
[24] X. Cheng, Y. Shen, L. Zhang, X. Liu, Philos. Mag. Lett. 92 (2012) 270.
[25] C.R. Weinberger, Phys. Rev. Lett. 105 (2010) 99601.
[26] C.R. Weinberger, Acta Mater. 58 (2010) 6535.
[27] Y. Liu, E. Van der Giessen, A. Needleman, Int. J. Solids Struct. 44 (2007) 1719.
[28] T.A. Khraishi, H.M. Zbib, J. Eng. Mater. Technol. Trans. ASME 124 (2002) 342.
[29] A.A. Kohnert, H. Tummala, R.A. Lebensohn, C.N. Tomé, L. Capolungo, Scr. Mater. 178 (2020) 161.
[30] J.C. Crone, L.B. Munday, J. Knap, Acta Mater 101 (2015) 40.
[31] D.M. Barnett, J. Lothe, J. Phys. Met. Phys. (1974) 4.
[32] A. Datta, A. Srirangarajan, U.V. Waghmare, U. Ramamurty, A.C. To, Comput. Mater. Sci. 50 (2011) 3342.
[33] M. Arul Kumar, A.K. Kanjarla, S.R. Niezgoda, R.A. Lebensohn, C.N. Tomé, Acta Mater. 84 (2015) 349.
[34] M. Arul Kumar, I.J. Beyerlein, C.N. Tomé, Acta Mater. 116 (2016) 143.
[35] R.A. Lebensohn, A.K. Kanjarla, P. Eisenlohr, Int. J. Plast. 59 (2012) 32–33.
[36] A.K. Kanjarla, R.A. Lebensohn, L. Balogh, C.N. Tomé, Acta Mater. 60 (2012) 3094.
[37] R.A. Lebensohn, Acta Mater. 49 (2001) 2723.
[38] M. Arul Kumar, I.J. Beyerlein, R.A. Lebensohn, C.N. Tomé, Model. Simul. Mater. Sci. Eng. (2017) 25.
[39] M. Arul Kumar, I.J. Beyerlein, R.J. McCabe, C.N. Tomé, Nat. Commun. 7 (2016) 13826.
[40] M. Arul Kumar, B. Leu, P. Rottmann, I.J. Beyerlein, TMS Magnesium Technology (2019) 2007.
[41] J.W. Zhang, B. Leu, M.A. Kumar, I.J. Beyerlein, W.Z. Han, Mater. Res. Lett. 8 (2020) 307.
[42] G. Simmons, H. Wang, Single Crystal Elastic Constants and Calculated Aggregate Progress, 2nd ed., M.I.T. Press, 34. The, 1965.
[43] I.J. Beyerlein, R.J. Mccabe, C.N. Tome, J. Mech. Phys. Solids 59 (2011) 988.
[44] M. Wronski, M. Arul Kumar, L. Capolungo, R.J. McCabe, K. Wierzbanowski, C.N. Tomé, Mater. Sci. Eng. A 724 (2018) 289.
[45] Y. Zhu, X. Wu, Mater. Res. Lett. 7 (2019) 393.
[46] M. Arul Kumar, I.J. Beyerlein, C.N. Tomé, J. Appl. Phys. (2016) 120.
[47] M.R. Barnett, M.D. Nave, A. Ghaderi, Acta Mater 60 (2012) 1433.
[48] B. Clausen, C.N. Tomé, D.W. Brown, S.R. Agnew, Acta Mater. 56 (2008) 2456.
[49] L. Jiang, et al., Mater. Sci. Eng. A 759 (2019) 142.
[50] Q. Sun, X.Y. Zhang, Y. Ren, J. Tu, Q. Liu, Scr. Mater. 90 (2014) 41.
[51] Q. Sun, X.Y. Zhang, J. Tu, Y. Ren, H. Qin, Q. Liu, Philos. Mag. Lett. 95 (2015) 145.
[52] Y. Liu, et al., Nat. Commun. 7 (2016) 8.
[53] Y. Liu, P.Z. Tang, M.Y. Gong, R.J. McCabe, J. Wang, C.N. Tomé, Nat. Commun. 10 (2019) 1.
[54] J. Tu, X.Y. Zhang, Z.M. Zhou, C. Huang, Mater. Charact. 110 (2015) 39.
[55] M. Gong, J.P. Hirth, Y. Liu, Y. Shen, J. Wang, Mater. Res. Lett. 5 (2017) 449.
[56] K. Dang, S. Wang, M. Gong, R.J. McCabe, J. Wang, L. Capolungo, Acta Mater. 185 (2020) 119.
[57] T. Braisaz, P. Ruterana, G. Nouet, R.C. Pond, Philos. Mag. A 75 (1997) 1075.
[58] H. El Kadiri, C.D. Barrett, J. Wang, C.N. Tomé, Acta Mater. 85 (2015) 354.
[59] C.D. Barrett, H. El Kadiri, Acta Mater. 70 (2014) 137.
[60] A. Ostapovets, R. Gröger, Model. Simul. Mater. Sci. Eng. (2014) 22.
[61] M. Gong, G. Liu, J. Wang, L. Capolungo, C.N. Tomé, Acta Mater. 155 (2018) 187.
[62] J. McGrath, C. Davis, J. Mater. Process. Technol. 666 (2004) 153–154.